NANO LETTERS

Letter

pubs.acs.org/NanoLett

Launching Propagating Surface Plasmon Polaritons by a Single Carbon Nanotube Dipolar Emitter

Nicolai Hartmann,[†] Giovanni Piredda,[†] Johann Berthelot,[‡] Gérard Colas des Francs,[‡] Alexandre Bouhelier,[‡] and Achim Hartschuh*,[†]

[†]Department Chemie and CeNS, Ludwig-Maximilians-Universität München, 81377 München, Germany

[‡]Laboratoire Interdisciplinaire Carnot de Bourgogne, CNRS UMR 5209, Université de Bourgogne, 9 Avenue Alain Savary, Dijon, France

Supporting Information

ABSTRACT: We report on the excitation of propagating surface plasmon polaritons in thin metal films by a single emitter. Upon excitation in the visible regime, individual semiconducting single-walled carbon nanotubes are shown to act as directional near-infrared point dipole sources launching propagating surface plasmons mainly along the direction of the nanotube axis. Plasmon excitation and propagation is monitored in Fourier and real space by leakage radiation microscopy and is modeled by rigorous theoretical calculations. Coupling to plasmons almost completely reshapes the emission of nanotubes both spatially and with respect to polarization as compared to photoluminescence on a dielectric substrate.

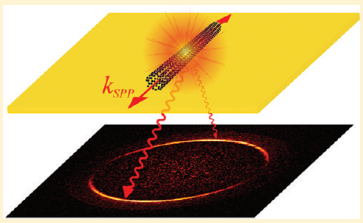

KEYWORDS: *Surface plasmons, single-walled carbon nanotubes, photoluminescence, radiation pattern imaging, leakage radiation microscopy*

Propagating surface plasmon polaritons (SPPs), electromagnetic waves bound to a metal−dielectric interface, have been studied extensively in the last decades.[1] SPPs provide the basis for nanophotonics, a very active research area aiming at optical device miniaturization and the integration of optics and electronics on a single chip. A series of passive two-dimensional (2D) SPP devices, such as beam splitters, mirrors, and concentrators have already been demonstrated.[2] SPPs, however, cannot be excited directly by propagating light waves due to the momentum mismatch between photons and plasmons. Different schemes coupling laser light to SPPs have been developed including the well-known Kretschmann configuration, Rayleigh scattering at nanoparticles,[3] near-field probes,[4] and tightly focused laser beams.[5] Alternatively, SPPs can be excited by the emission of quantum systems positioned in close proximity to metal films and has been demonstrated for dye molecules and semiconductor nanocrystals.[6,7] These SPP sources could be integrated directly into 2D circuitry and could also serve as gain media in active elements.[8] Electrical contacting and excitation of such single SPP sources, however, would be extremely challenging and external optical pumping would still be required. Ideally, SPP sources would operate in the near-infrared (NIR) spectral region to exploit the long propagation length of plasmons in this regime and to minimize losses. Moreover, efficient coupling of SPPs to functional elements, for example for focusing,[9,10] refraction,[11] and guiding,[12] requires the directional excitation of plasmons.

In this manuscript, we report on the directional excitation of propagating surface plasmon polaritons on a thin metal film by individual single-walled carbon nanotubes (SWCNTs). The investigation of single emitters avoids ensemble averaging of orientations and emission energies, which is of particular importance in the case of nanotubes because of their structural diversity, and provides access to the quantum properties of the emission. Upon laser excitation in the visible photoluminescent SWCNTs launch SPPs in the NIR propagating for several micrometers predominately in the direction of the nanotube axis. SPP excitation and propagation are investigated by leakage radiation microscopy[13−15] in real and Fourier space. Polarized radiation patterns recorded for single SWCNTs on gold films reveal an almost complete redistribution of the angular emission with respect to SWCNTs on glass resulting in highly directive PL emission lobes. The observed emission characteristics of the nanotubes are also in marked difference to the case of coupling to localized radiating surface plasmons in a sharp metal tip antenna studied previously.[16] Rigorous model calculations of spatial intensity distributions and radiation patterns show that plasmon excitation results from radiating point dipole sources. The observed directionality and long propagation length together with the well-controlled emission spectra of SWCNTs and the possibility of electrical excitation of emission[17,18] makes them promising candidates as functional elements in nanophotonic devices.

We used an inverted confocal microscope with an oil immersion objective (NA = 1.4) and a linearly polarized diode laser running at λ_{exc} = 565 nm for excitation. The setup can be operated in three different detection configurations: (1)

Received: September 19, 2011
Revised: December 9, 2011
Published: December 16, 2011

   dx.doi.org/10.1021/nl203270b | *Nano Lett.* 2012, 12, 177−181

scanning confocal imaging with an avalanche photodiode (APD), (2) Fourier space imaging (Figure 1a) and (3) wide-field real space imaging (Figure 1b). A CCD camera is used to record both Fourier and real space images.

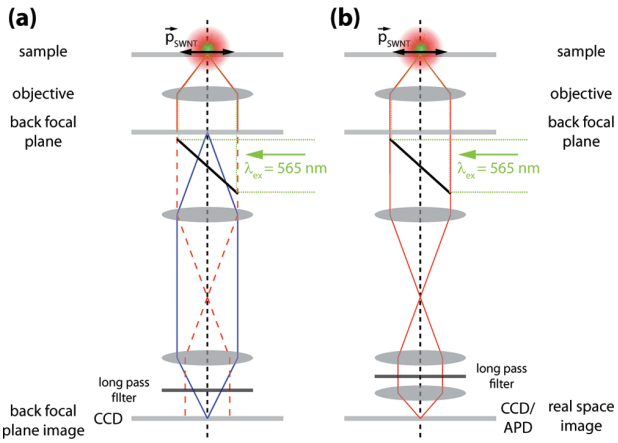

Figure 1. Schematic of the experimental setup. Three different imaging and detection methods were used after confocal laser excitation at λ_{exc} = 565 nm. (a) Fourier (back focal plane) imaging by a CCD camera. (b) Real space imaging by a CCD camera and scanning confocal detection using an APD.

The samples consist of 25 nm thick gold films, evaporated onto thin microscope glass cover slides (Figure 2). On top of

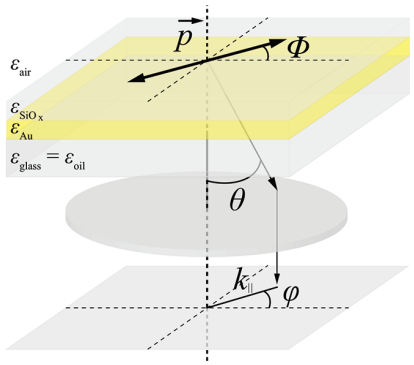

Figure 2. Schematic of the multilayer structure and the coordinate system.

the metal film, an additional SiO_x spacer layer with a thickness of 35 ± 5 nm was evaporated to prevent quenching of the SWCNT PL via coupling to nonradiative lossy modes in the metal.[19,20] One milligram of raw HiPCO SWCNTs (as purchased from Unidym Inc.) per mL 1 wt % sodium deoxycholate (SDC, Sigma-Aldrich Inc.) solution in water were dispersed by sonication over 3 h. After centrifugation to remove bundles, a diluted solution of the supernatant SWCNT dispersion was spin-coated on top of the metal samples. Because the unsorted HiPCO material contains several nanotube chiralities, a 950 nm long-pass filter was used for all detection methods. Together with the diminishing detection efficiency of the CCD camera for wavelengths above 1010 nm, PL detection is limited to a spectral window ranging from 950 to 1010 nm. This spectral window selects the emission of (6,5) SWCNTs. Since its E22 transition matches the photon energy of the laser source this SWCNT species is excited most efficiently in our experiment.

We base all of our calculations on the transfer matrix method, as our samples are accurately represented by a multilayer structure.[21] The wavenumber and propagation length of the plasmons that propagate freely at the gold−SiO_x interface of our samples are calculated by setting the appropriate element of the characteristic matrix of the multilayer structure to zero.[22] The calculations of the Fourier plane and real space images follow the treatment of ref 23 (for more details see Supporting Information).

As a first step the samples were imaged by scanning confocal PL microscopy to locate (6,5) SWCNTs (Figure 3a). In the confocal image, the SWCNTs appear as luminescent spots. This is expected since the raw material contains rather short nanotubes that are cut further by sonication. Next we recorded the Fourier plane radiation pattern (Figure 3b−d) and the real space image (Figure 3e−g) of each SWCNT we identified in the PL image.

The most prominent characteristic of the Fourier plane images (Figure 3b−d) is the confinement of the emission to a very narrow angular range. The observed rings are the signatures of plasmons radiating into the substrate.[24] The radius of the rings is determined by the resonance condition between SPPs bound to the SiO_x−gold interface and photons in the lower halfspace with higher refractive index (n_{oil},n_{glass}). Because momentum conservation plasmons can only couple to photons with equal in-plane momentum $k_{SPP} = k_{||}$.

The fact that the rings are not continuous and only bright arcs are observed shows the directional excitation of the SPPs by a polarized source, that is, the emitting nanotube. Directional propagation of the SPPs after local excitation is evident in the corresponding real space images (Figure 3e−g) recorded at the same positions that show an elongated spatial distribution of the emission indicating a propagation length of several micrometers.

For nanotubes, the strongest optical transitions as well as the PL emission are polarized along the nanotube axis.[25] Since the polarization of the exciting laser was vertical, as indicated by the arrow in (Figure 3a), only SWCNTs oriented parallel to this direction could be excited efficiently and are observed. From both real and Fourier space images in Figure 3, we can thus conclude that SPPs are launched mainly in the direction of the SWCNT axis. In addition, no horizontally oriented real and Fourier space patterns could be detected which is a clear indication that nanotube orientation and plasmon propagation direction coincide. This conclusion is further supported by excitation polarization dependent PL and atomic force microscopy images together with the radiation patterns recorded for the same nanotubes that are included as Figures S1 and S2 of the Supporting Information.

In the following, we model the observed Fourier and real space images theoretically, quantify the plasmon propagation length L_{SPP} and examine the mechanism of plasmon excitation. An asymptotic expression for the surface plasmon fields for a single in-plane dipole is given in ref 26 as

$$E(r, \phi) \propto \cos(\phi)\frac{1}{\sqrt{r}}E_0 e^{i\{k_{SPP}+i[1/(2L_{SPP})]\}r} \quad (1)$$

The Fourier pattern rendered by a single dipole can then be calculated directly as the modulus square of the Fourier transform of eq 1. Since no analytical expression for the Fourier transform of eq 1 is available, we used a Lorentzian line shape

dx.doi.org/10.1021/nl203270b | Nano Lett. 2012, 12, 177−181

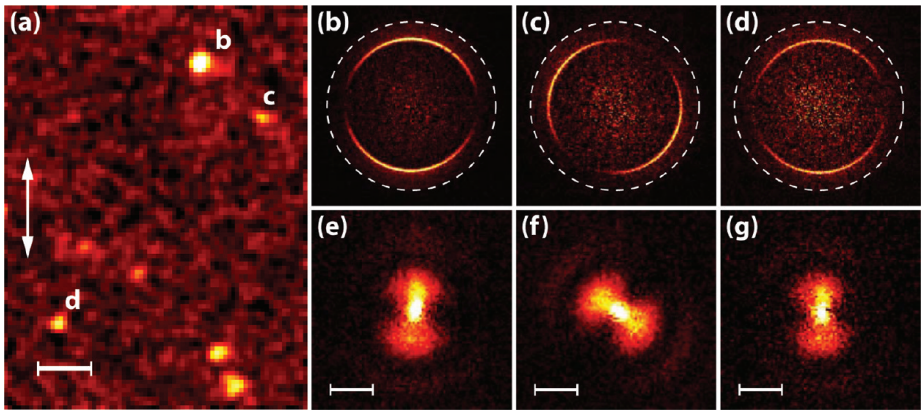

Figure 3. (a) Confocal PL image of single SWCNTs on a 35 nm SiO_x spacer layer on top of a 25 nm gold film. The scale bar represents 2.0 μm. The laser polarization, indicated by the white arrow, selects mainly nanotubes with vertical in-plane orientation. Launching of SPPs upon local laser excitation is shown for three SWCNTs marked in (a) by b, c, and d. In the Fourier (k-) space images of these nanotubes (b–d) SPP excitation renders sharp arcs formed by photons with in-plane momentum $k_{\|}$ matching the plasmon momentum k_{SPP}. The dashed circle marks the numerical aperture of the objective (NA = 1.4). In the corresponding real space images (e–g), SPP propagation leads to a double lobe structure extending several micrometers away from the central excitation spot. The scale bar represents 4.0 μm. The same directivity of plasmon excitation is seen in the corresponding Fourier and real space images (b and e, c and f, and d and g, respectively). Plasmons are launched predominately in the direction of the SWCNTs.

function as an approximation for fitting of the experimental data[27] (for more details see Figure S3 of the Supporting Information)

$$I(k_{\|}, \phi) = y_0 + I_0 \frac{\cos^2(\phi - \Phi)}{(k_{\|} - k_{SPP})^2 + (2L_{SPP})^{-2}} \quad (2)$$

Here y_0 denotes the contribution of a background, I_0 is the amplitude, Φ is the in-plane orientational angle of the dipole corresponding to the direction of the SWCNT axis, k_{SPP} determines the position of the maximum of the emission ring corresponding to the plasmon resonance condition $k_{SPP} = k_{\|}$ and L_{SPP} is the propagation length of the SPPs. Figure 4 depicts

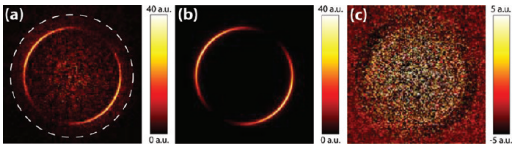

Figure 4. (a) Experimentally obtained Fourier plane pattern from a single photoluminescent SWCNT on a 35 nm SiO_x spacer layer on top of a 25 nm gold film. The dashed circle marks the numerical aperture of the objective (NA = 1.4). (b) Fit of (a) according to eq 2 assuming a single in-plane dipole source. (c) Residuum after subtraction (b − a). The fit yields a surface plasmon propagation length of $L_{SPP} = 4.2 \pm 0.1$ μm.

a representative example where the experimentally obtained Fourier pattern was fitted according to eq 2 with the resulting residuum after subtracting the experimental from the best-fit pattern.

The Fourier image was calibrated with the maximum **k**-vector $\mathbf{k}_{max}$ corresponding to the NA of the microscope objective. From the fit we then extract the plasmon momentum k_{SPP} or the angle of the emitted leakage radiation $\theta_{SPP} = \arcsin(k_{SPP}/(k_0 n_{glass}))$ and the propagation length L_{SPP}.

To compare our experimental results with theoretical predictions we calculated θ_{SPP} and L_{SPP} numerically using the transfer matrix method.[22] The experimental values for the emission angle $\theta_{SPP} = 45.9 \pm 0.2°$ and the propagation length of $L_{SPP} = 4.2$ μm $\pm$ 0.1 μm are reproduced with good agreement by the calculation ($\theta_{SPP} = 44.6°$ and $L_{SPP} = 4.7$ μm). For the calculation, we used the dielectric constant of gold at 980 nm from ref 28, a refractive index of SiO_x of $n_{SiO_x} = 1.5$ and the measured thicknesses of the gold and the SiO_x layers (24 and 35 nm, respectively). The spectral width of the nanotube PL of about 50 meV translates into a small angular broadening of the measured emission arcs due to the dispersion relation of gold which leads to a spread of the resonance angle by 0.1°. This results in an underestimation of the actual propagation length by about 500 nm. The discrepancy between experimental and theoretical plasmon angle θ_{SPP} of 1.3°, however, is larger than the accuracy of our measurement. After sample preparation, residual SDC surfactant remains on top of the SiO_x spacer layer and around the SWCNTs that is likely to increase the effective refractive index as compared to air. Considering this by setting the refractive index of the upper medium to $n_{air} = 1.023$ in the calculation reproduces the experimentally observed plasmon angle exactly.

Note that in the present configuration the propagation length is mainly limited through coupling to leakage radiation that we used to study the SPPs. For thicker gold films exceeding 70 nm, this coupling would be negligible. Keeping the spacer layer thickness of 35 nm would then result in a propagation length on the order of 40 μm.

Real space images of single dipole emitters were calculated by Fourier transformation of the angular spectrum of the electromagnetic field at the gold/glass interface created by a single in-plane dipole using the imaging properties of our microscope (for more details see Supporting Information). Figure 5a shows an experimental real space image rendered by a single SWCNT after focused excitation and Figure 5b the calculated intensity distribution of a single emitter on a 35 nm SiO_x spacer layer on top of a 25 nm gold film. The shape of the real space pattern, in particular its double lobe structure and the weak diffractions rings at larger distances from the nanotube, is reproduced well. The size of the pattern, on the other hand, depends sensitively on the effective NA of the microscope

dx.doi.org/10.1021/nl203270b | *Nano Lett.* 2012, 12, 177–181

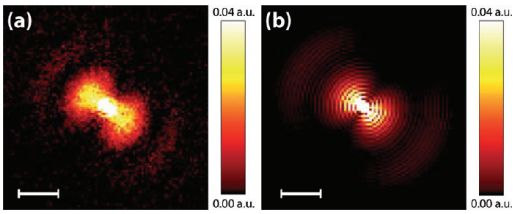

Figure 5. (a) Experimental real space image rendered by a single photoluminescent SWCNT on a 35 nm SiO_x spacer layer on top of a 25 nm gold film. (b) Theoretical image of an in-plane dipole oriented along the nanotube axis. The scale bar represents 4.0 μm in (a) and (b). Both images are normalized to one and the color scale is saturated at 0.04 to allow for an examination of their low intensity details.

objective that is known to be reduced by the lower transmission factors of the marginal rays.[29] In the calculation, we used an effective NA of 1.25. (For comparison we included the corresponding image for NA = 1.4 as Figure S4 in the Supporting Information.) In general, we find that the values for the surface plasmon propagation length L_{SPP} obtained from real space images are affected by large uncertainties due to the effect of the NA and the more complex spatial dependence of the intensity following eq 1. Importantly, while the lower transmission of the marginal rays leads to reduced signal intensities in the Fourier-plane image, it does not affect their angular distribution observed in Figure 4. This underlines the advantages of Fourier-plane imaging for analyzing SPP excitation and the quantification of the propagation length.

The good agreement between the theoretical images calculated for a single dipole and the experimental images observed for SWCNTs shows that nanotubes act as dipolar sources for plasmons propagating mainly in the direction of the nanotube axis. In essence, exciton recombination in nanotubes launches propagating surface plasmons on the metal film. These plasmons can couple to photon modes in the lower halfspace that are finally detected as leakage radiation.

Coupling to plasmons almost completely reshapes the emission of nanotubes both spatially and with respect to polarization as compared to PL emission on dielectrics. In Figure 6, polarization resolved radiation patterns of single SWCNTs on glass (a–c) and on SPP supporting metal films (g–i) are presented. Also shown are the corresponding theoretical patterns calculated for single dipole emitter on glass (d–f) and metal film (j–l), respectively (for more details on the calculations see Supporting Information). As the only free parameter the dipole orientation has been adjusted to match the measured patterns without analyzer indicated by the arrows in Figure 6d,j, respectively.

On glass, the PL is distributed over a large angular range with highest intensities occurring in the directions perpendicular to the nanotube axis resulting in two broad lobes with a maximum peaking near the critical angle (Figure 6a). The PL pattern of the same SWCNT recorded with vertical and horizontal analyzer orientations and the corresponding emission patterns are also shown. The PL is polarized mainly parallel to the dipole orientation (Figure 6b,e). Remarkably, a single emitter also leads to a substantial orthogonal component as can be seen both from theory and experiment (Figure 6c,f).

In contrast, the emission patterns from SWCNTs on a metal film (Figure 6g–i) show emission concentrated around the direction of the dipole. The polarization is seen to vary spatially both in the experimental and the theoretical pattern (Figure

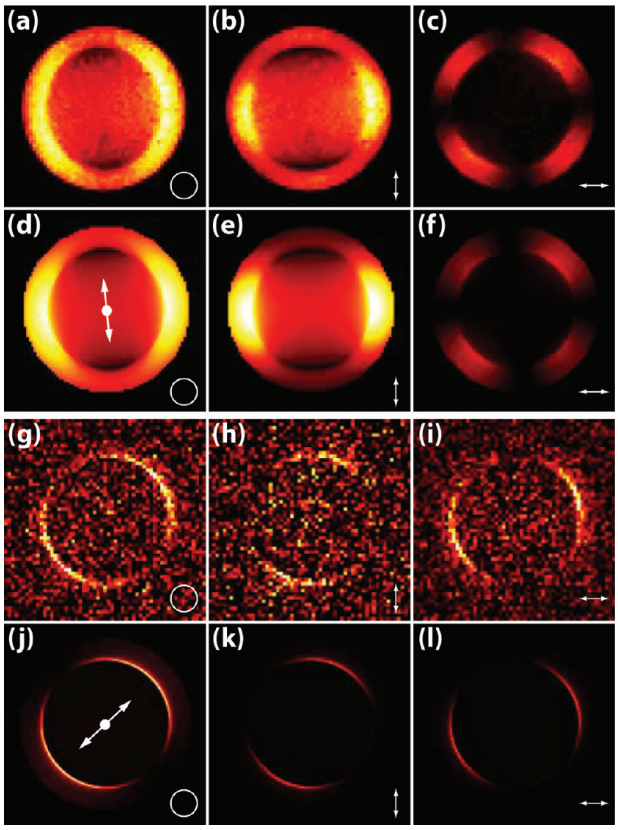

Figure 6. Comparison between experimentally obtained and calculated Fourier patterns with different polarizations for a SWCNT deposited on glass: (a,d) without analyzer, (b,e) analyzed vertically, and (c,f) analyzed horizontally. The corresponding images for a SWCNT on a 25 nm gold film: (g,j) without analyzer, (h,k) analyzed vertically, and (i,l) analyzed horizontally. The white arrow in the theoretical images (d) and (j) indicates the direction of the point dipole used for the calculations.

6h,i and k,l, respectively). At every point the polarization is oriented along the direction of plasmon propagation. In other words, the polarization is radial with respect to the origin formed by the position of the dipolar plasmon source as derived in ref 26 (eq 18) and described in ref 30. This clearly confirms that SPPs are launched mainly in the direction of the dipole and therefore in the direction of the SWCNT.

The plasmon-induced narrowing of the PL emission can be quantified by calculating the maximum effective directivity $D^{eff}_{max} = p_{max}(1.51\pi/P_{rad})$ for nanotubes on gold films and on glass using the measured and theoretically calculated radiation patterns.[31] Here the peak intensity p_{max} is compared to the average intensity P_{rad} detected within the accessible angular range 1.51π steradian. From the experimental data shown in Figure 6, we determine a maximum effective directivity on glass of $D^{eff}_{max} = 9$, which is in good agreement with the theoretical value of $D^{eff}_{max} = 10$. Plasmon coupling leads to a substantially increased maximum effective directivity of $D^{eff}_{max} = 55$ (experiment) and $D^{eff}_{max} = 74$ (theory).

In summary, we reported the excitation of propagating surface plasmon polaritons by single optically excited semiconducting single-walled carbon nanotubes. Leakage radiation microscopy images in Fourier and real space recorded for the same nanotubes revealed the propagation length and direction

dx.doi.org/10.1021/nl203270b | *Nano Lett.* 2012, 12, 177–181

of SPPs. Our results demonstrate that nanotubes can act as SPP sources making them promising candidates for integration in plasmonic and nanophotonic circuits. Moreover, combining surface plasmon coupling with electroluminescence from carbon nanotubes opens up the possibility to create an efficient electrically driven nanoscale plasmon source.

■ ASSOCIATED CONTENT

Supporting Information

Detailed description of theorectical calculation of Fourier and real space images. Excitation polarization dependence of PL images and radiation patterns (Figure S1). Atomic force microscopy topography image and radiation pattern recorded for the same nanotubes (Figure S2). Comparison between the curve obtained taking the modulus square of the Fourier transform of eq 1 and a Lorentzian line shape function according to eq 2 (Figure S3). Calculated real space image rendered by a single in-plane dipole using NA = 1.4 (Figure S4). This material is available free of charge via the Internet at http://pubs.acs.org.

■ AUTHOR INFORMATION

Corresponding Author

*E-mail: achim.hartschuh@cup.uni-muenchen.de.

■ ACKNOWLEDGMENTS

The authors acknowledge Sabrina Schwindl and Harald Budde (both LMU) for experimental support. This work was funded by the Nanoscience Europe (E2-Plas) and the DFG through HA4405/5-1 and the Nanosystems Initiative Munich (NIM).

■ REFERENCES

(1) Raether, H. *Surface Plasmons on Smooth and Rough Surfaces and on Gratings*; Springer: New York, 1986.
(2) Hohenau, A.; Krenn, J. R.; Stepanov, a. L.; Drezet, A.; Ditlbacher, H.; Steinberger, B.; Leitner, A.; Aussenegg, F. R. *Opt. Lett.* **2005**, *30*, 893−895.
(3) Ditlbacher, H.; Krenn, J.; Felidj, N.; Lamprecht, B.; Schider, G.; Salerno, M.; Leitner, A.; Aussenegg, F. R. *Appl. Phys. Lett.* **2002**, *80*, 404−6.
(4) Hecht, B.; Bielefeldt, H.; Novotny, L.; Inouye, Y.; Pohl, D. W. *Phys. Rev. Lett.* **1996**, *77*, 1889−92.
(5) Bouhelier, A.; Ignatovich, F.; Bruyant, A.; Huang, C.; Colas des Francs, G.; Weeber, J.-C.; Dereux, A.; Wiederrecht, G. P.; Novotny, L. *Opt. Lett.* **2007**, *32*, 2535−2537.
(6) Lakowicz, J. R.; Ray, K.; Chowdhury, M.; Szmacinski, H.; Fu, Y.; Zhang, J.; Nowaczyk, K. *Analyst* **2008**, *133*, 1308−46.
(7) Gryczynski, I.; Malicka, J.; Jiang, W.; Fischer, H.; Chan, W. C. W.; Gryczynski, Z.; Grudzinski, W.; Lakowicz, J. R. *J. Phys. Chem. B* **2005**, *109*, 1088−93.
(8) Grandidier, J.; Colas des Francs, G.; Massenot, S.; Bouhelier, A.; Markey, L.; Weeber, J.-C.; Finot, C.; Dereux, A. *Nano Lett.* **2009**, *9*, 2935−2939.
(9) Schuller, J. a.; Barnard, E. S.; Cai, W.; Jun, Y. C.; White, J. S.; Brongersma, M. L. *Nat. Mater.* **2010**, *9*, 193−204.
(10) Yin, L.; Vlasko-Vlasov, V. K.; Pearson, J.; Hiller, J. M.; Hua, J.; Welp, U.; Brown, D. E.; Kimball, C. W. *Nano Lett.* **2005**, *5*, 1399−402.
(11) Hohenau, A.; Krenn, J. R.; Stepanov, A. L.; Drezet, A.; Ditlbacher, H.; Steinberger, B.; Leitner, A.; Aussenegg, F. R. *Opt. Lett.* **2005**, *30*, 893−5.
(12) Gramotnev, D. K.; Bozhevolnyi, S. I. *Nat. Photonics* **2010**, *4*, 83−91.
(13) Bouhelier, A.; Huser, T.; Tamaru, H.; Güntherodt, H.-J.; Pohl, D. W. *Phys. Rev. B* **2001**, *63*, 155404−13.
(14) Calander, N. *Anal. Chem.* **2004**, *76*, 2168−73.
(15) Zhang, D. G.; Moh, K. J.; Yuan, X. C. *Opt. Express* **2010**, *18*, 12185−12185.
(16) Böhmler, M.; Hartmann, N.; Georgi, C.; Hennrich, F.; Green, A. A.; Hersam, M. C.; Hartschuh, A. *Opt. Express* **2010**, *18*, 16443−51.
(17) Freitag, M.; Chen, J.; Tersoff, J.; Tsang, J. C.; Fu, Q.; Liu, J.; Avouris, P. *Phys. Rev. Lett.* **2004**, *93*, 076803−4.
(18) Avouris, P.; Freitag, M.; Perebeinos, V. *Nat. Photonics* **2008**, *2*, 341−50.
(19) Fort, E.; Grésillon, S. *J. Phys. D: Appl. Phys.* **2008**, *41*, 013001−31.
(20) Vasilev, K.; Knoll, W.; Kreiter, M. *J. Chem. Phys.* **2004**, *120*, 3439−45.
(21) Born, M. Wolf, E. *Principles of optics*, 6th ed.; Pergamon: Oxford, 1970.
(22) Walpita, L. M. *J. Opt. Soc. Am. A* **1985**, *2*, 595−602.
(23) Novotny, L.; Hecht, B. *Principles of Nano-Optics*; Cambridge University Press, New York, 2008.
(24) Drezet, A.; Hohenau, A.; Koller, D.; Stepanov, A.; Ditlbacher, H.; Steinberger, B.; Aussenegg, F. R.; Leitner, A.; Krenn, J. R. *Mater. Sci. Eng., B* **2008**, *149*, 220−229.
(25) *Carbon Nanotubes*; Jorio, A., Dresselhaus, M. S., Dresselhaus, G., Eds.; Springer: Berlin/Heidelberg, 2008; Vol. *111*.
(26) Archambault, A.; Teperik, T. V.; Marquier, F.; Greffet, J. J. *Phys. Rev. B* **2009**, *79*, 195414−22.
(27) Colas des Francs, G.; Grandidier, J.; Massenot, S.; Bouhelier, A.; Weeber, J.-C.; Dereux, A. *Phys. Rev. B* **2009**, *80*, 115419.
(28) Johnson, P. B.; Christy, R. W. *Phys. Rev. B* **1972**, *6*, 4370−4379.
(29) Tang, W. T.; Chung, E.; Kim, Y. H.; So, P. T. C.; Sheppard, C. J. R. *Opt. Express* **2007**, *15*, 4634−4646.
(30) Lakowicz, J. R. *Anal. Biochem.* **2004**, *324*, 153−169.
(31) Bharadwaj, P.; Deutsch, B.; Novotny, L. *Adv. Opt. Photon.* **2009**, *1*, 438−483.

Supplementary Information for

Launching Propagating Surface Plasmon Polaritons by a Single Carbon Nanotube Dipolar Emitter

Nicolai Hartmann, [†] Giovanni Piredda, [†] Johann Berthelot[‡], Gérard Colas des Fancs[‡], Alexandre Bouhelier, [‡] and Achim Hartschuh *,[†]

† Department Chemie and CeNS, Ludwig-Maximilians-Universität München, 81377 München, Germany

‡ Laboratoire Interdisciplinaire Carnot de Bourgogne, CNRS UMR 5209, Université de Bourgogne, 9 Avenue Alain Savary, Dijon, France

*E-mail: achim.hartschuh@cup.uni-muenchen.de

Theoretical calculations of Fourier plane and real space images

Radiation patterns can be obtained by splitting the angular representation of the dipole Green's function into its s- and p- polarized components and propagating each plane wave through the layered substrate using a matrix transfer method (ref. 18 in the paper: Walpita, L. M. *J. Opt. Soc. Am. A* **1985**, *2*, 595–602); far-fields can be calculated from the angular spectrum obtained in this way by multiplication with a cosine factor and finally the field distribution in the Fourier plane of the imaging system can be obtained by mapping the components of the far-field expressed in spherical coordinates into a system of cylindrical coordinates. The procedure is explained in detail in [1].

The calculations of the field distributions follows the same principles; in this case the field components must be mapped from the spherical system of coordinates that corresponds to the so called "reference sphere" of the objective lens to a spherical system of coordinates corresponding to the reference sphere of the imaging lens; the calculations are carried out in [2] and we implemented their formulae substituting once more the proper transmission coefficients for the s- and p- polarized components.

Excitation polarization dependence of PL images and radiation patterns

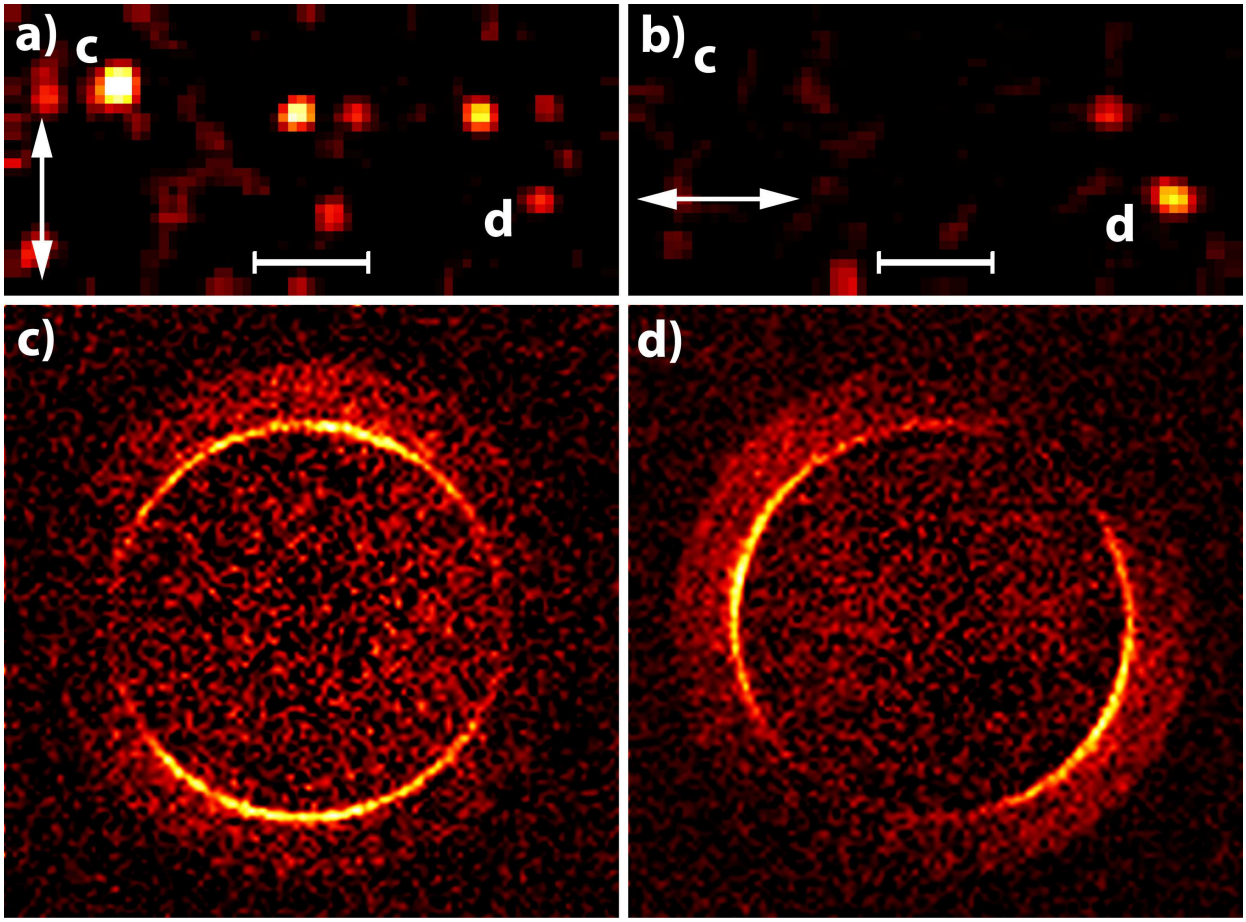

Figure S1: Confocal PL images of randomly oriented nanotubes on a dielectric / gold substrate recorded for vertical (a) and horizontal excitation polarization (b) as indicated by the direction of the arrows (scale bar 2 µm, same intensity scaling). (c) and (d) show the radiation patterns detected at the respective positions c and d marked in (a) and (b). The nanotube at position c that is excited only for vertical polarization is seen to launch propagating surface plasmons mainly in the same direction. In contrast, the nanotube at position d shows a stronger PL response for horizontal polarization and correspondingly, plasmon excitation occurs mainly in horizontal direction. The lower polarization contrast observed in the confocal images at position d results from the non-perfect horizontal orientation of this nanotube.

Atomic force microscopy images and radiation patterns of the same nanotubes

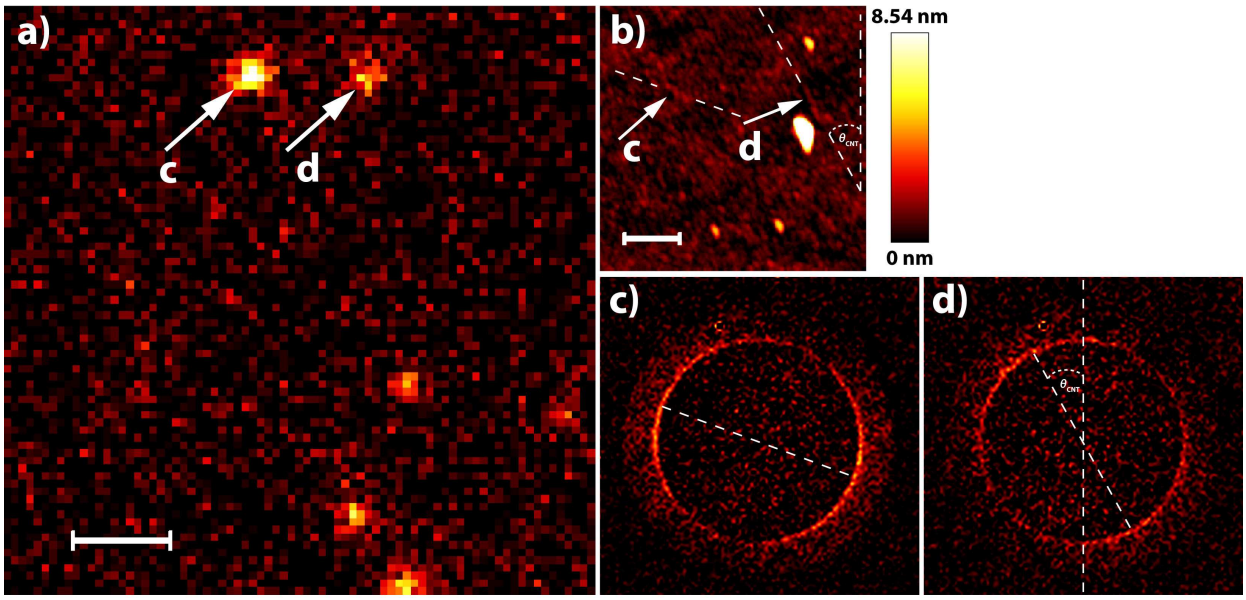

Figure S2: (a) Confocal PL image of nanotubes on a dielectric / gold substrate (scale bar 1 µm). (b) Atomic force microscopy image showing the two photoluminescent nanotubes at positions c and d marked by arrows in (a) (scale bar 300 nm). The identification of the thin nanotubes with diameter of around 0.8 nm is somewhat hindered by the surface roughness of the SiOx spacer layer. In the present case the identification is supported by the comparable nanotube position and separation seen in the PL and the AFM image. The radiation patterns recorded for the two differently oriented nanotubes at position c and d are shown in (c) and (d). The orientation of the nanotubes coincides with the direction of the plasmon excitation seen in (c) and (d).

Comparison between plasmon radiation pattern and Lorentzian approximation

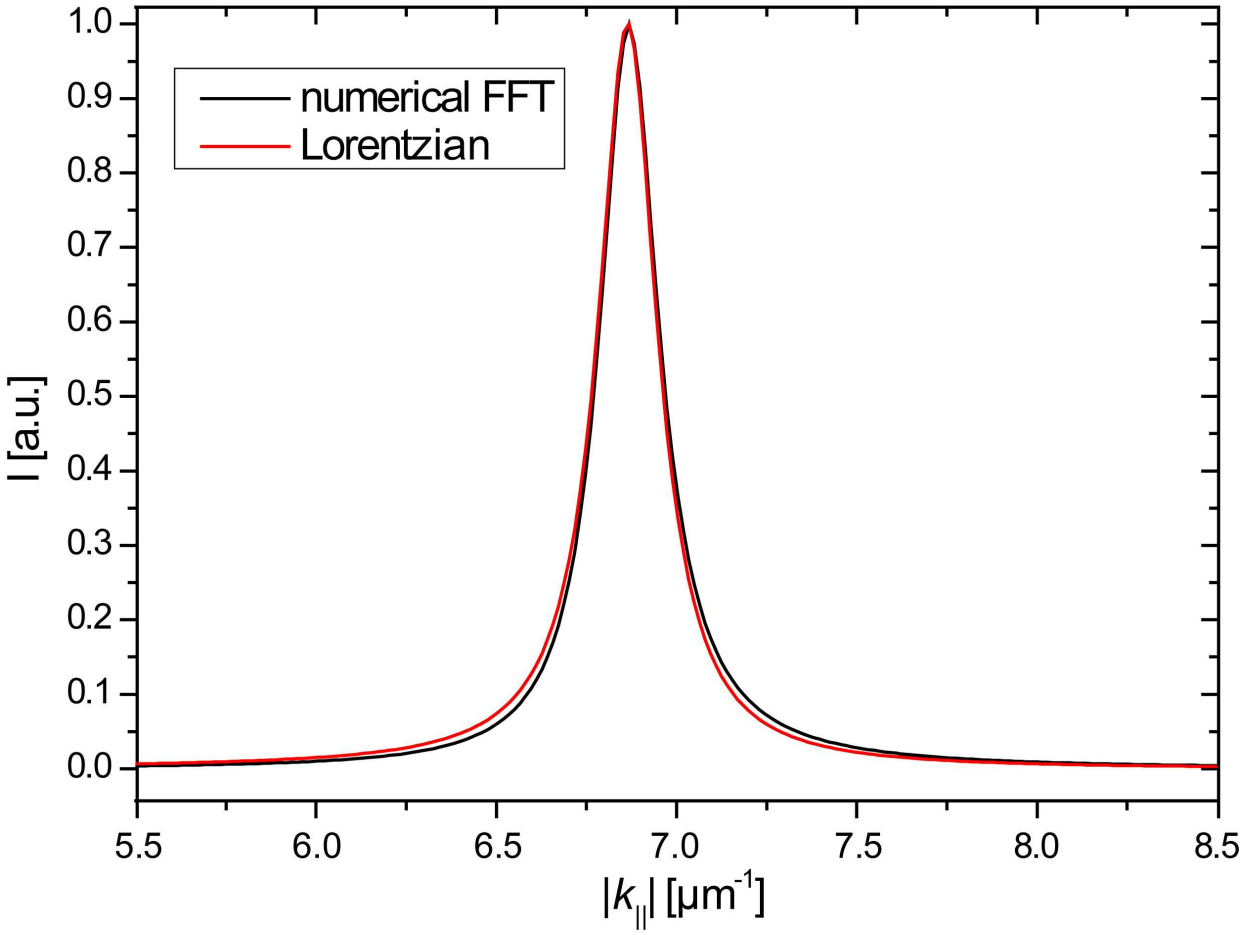

Figure S3: Comparison of the modulus square of the numerical Fourier transform of the asymptotic plasmon field (eqn. 1) according to [3] and a Lorentzian line shape function (eqn. 2) using the same plasmon propagation length L_{SPP}. The curves represent cross-sections obtained for $\varphi = 0$ ($\Phi = 0$). The Lorentzian line shape function represents a good approximation regarding both peak position and peak width

Real space image rendered by single in-plane dipole using NA = 1.4

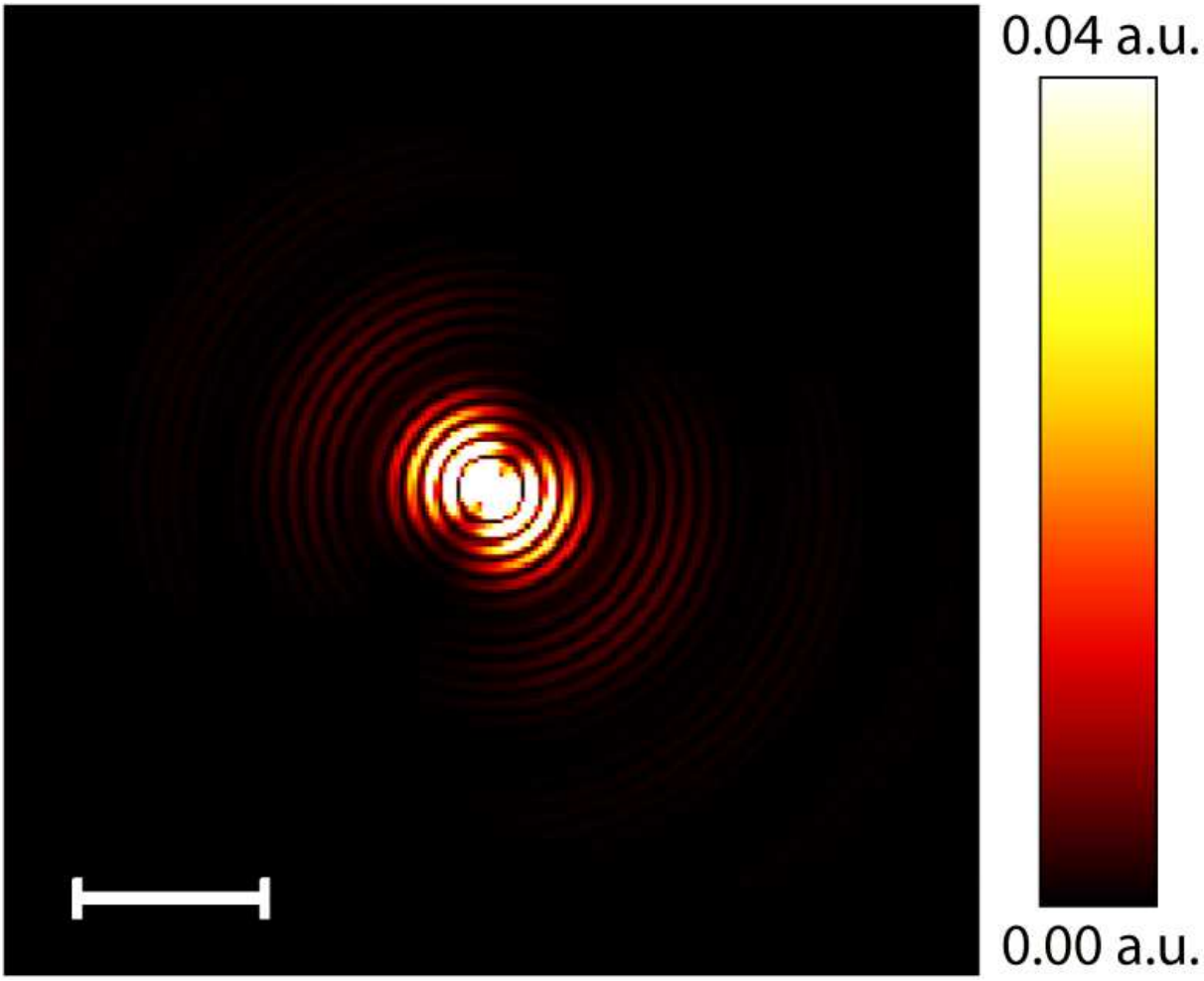

Figure S4: Calculated real space image rendered by a single in-plane dipole on a 35 nm SiO_x spacer layer on top of a 25 nm gold film using NA=1.4. The scale bar represents 4 µm.

[1] Novotny, L. and Hecht, B. *Principles of Nano-Optics*; Cambridge University Press, 2008.

[2] Tang, W. T. et al. *Opt. Expr.* **2007**, 15, 4634-4646

[3] Archambault, A.; Teperik, T. V.; Marquier, F.; Greffet, J. J. *Phys. Rev. B* **2009**, 79 , 195414–22.